AXISYMMETRIC AND CYLINDRICAL ISOSTABILOIDS

by Peter R. Preiswerk, John M. Hedgepeth,
and Hans U. Schuerch

AXISYMMETRIC AND CYLINDRICAL ISOSTABILOIDS

By Peter R. Preiswerk, John M. Hedgepeth,
and Hans U. Schuerch

SUMMARY

The differential equations for the geometric layout of compression-loaded axisymmetric and cylindrical two-family filamentary structures are established. The analytical formulation is based upon the requirement that failure due to local instability occurs simultaneously in the whole structure.

Solutions are obtained for the particular case where the body force due to the structure's own weight is the only load. For this special case, the shapes of the meridian and the cross section, respectively, have been determined, as well as the pattern of the filaments. In addition, the weight per area covered by the structure is formulated and discussed. Minimum-weight configurations are defined. Examples for large earth-based and moon-based structures are presented.

LIST OF ILLUSTRATIONS

INTRODUCTION

Among high-performance structures maximum economy of material is often obtained by a design in which all structural components fail simultaneously as the structure is subjected to a unique ultimate loading condition. Examples of such structures are the uniformly stressed Maxwell-Michell type networks, isotropically stressed structural "soap-film" membranes, uniformly stressed filamentary network structures ("isotensoids")(Refs. 1, 2), and the "Shanley tube" (Ref. 3), which is designed to fail simultaneously in a local and general instability mode.

Analogously to the isotensoids, structures can be found which are uniformly compressed. These "isocompressoids" are the subject of a recent study (Ref. 4). However, under compressive loads, failure of the structure due to instability may occur long before the compressive stress limit is reached. The present report treats this stability problem from a standpoint of buckling of the individual structural members. Hence, the analytical design condition imposed upon the structure is that each element buckle as an Euler column between network nodes upon reaching the design ultimate load. The term "isostabiloid" is used to describe the filamentary structural configurations satisfying this condition.

This analysis deals with axisymmetric and cylindrical configurations with axisymmetric (or uniform along the length) loadings. In either case no circumferential (or lengthwise) loadings are considered. The influences of general instability are recognized but only briefly discussed.

LIST OF SYMBOLS

A cross-sectional area of a single rod

b $= \sin^2 \beta_a$

C buckling end-fixity coefficient

D tube diameter

d, d_1, d_2 dimensions of particular Sintes column (Fig. 13)

E elasticity modulus

f_D, f_T weight form factors for gravity-loaded isostabiloids

$\overline{f}_D, \overline{f}_T$ stress form factors for gravity-loaded isostabiloids

g gravitational acceleration

h $= \sin^2 \beta$

I moment of inertia of rod cross section

k curvature at apex of structure in nondimensional coordinates

K_f stiffness form factor of rod cross section $\left(= \dfrac{I}{A^2} \right)$

m mass per unit planform area of gravity-loaded isostabiloids

n number of filaments in each family

$\overline{n}$ number of rod sections in each filament

N number of unrestrained filament intersections

p_m external meridional load per unit surface area

p_n external normal load per unit surface area

P_{cr} local buckling load of rod

q number of meridional node lines in general failure mode of axisymmetric shells

r	radial coordinate
R	nondimensional radial coordinate in gravity-loaded axisymmetric structure (see Eq. 5)
s	spacing of filaments at perimeter
t	wall thickness
x	widthwise coordinate in cylindrical structures
$\bar{X}$	nondimensional widthwise coordinate in gravity-loaded cylindrical structures (see Eq. 7)
y	axial coordinate in cylindrical structures
$\bar{Y}$	nondimensional axial coordinate in gravity-loaded cylindrical structures (see Eq. 7)
z	vertical coordinate
Z	nondimensional vertical coordinate in gravity-loaded axisymmetric structures (see Eq. 5)
$\bar{Z}$	nondimensional vertical coordinate in gravity-loaded cylindrical structures (see Eq. 7)
α	angle between meridian and vertical
β	angle between meridian and filament
$\Delta \ell$	length of filament between two intersections
ρ	density of rod material
σ	stress

Subscripts:

$\ldots_a$	values at apex of cylindrical structures
$\ldots_o$	values at rim of structure

BASIC RELATIONS

Axisymmetric Isostabiloid

Consider an axisymmetric structure consisting of two families of interconnected rods as the load-carrying parts, and built in such a way that the arrangement pattern of one family of rod trajectories is the reflected image of the other family. The rod trajectories are referred to as "filaments", indicating that these may be continuous structural members, connected to other filaments at localized points of intersection.

Let n be the number of filaments in each family; then the length of an element, $\Delta\ell$, between two intersections is, with the notation of Figure 1,

$$\Delta\ell = \frac{1}{2} \frac{2\pi r}{n} \frac{1}{\sin\beta} \tag{1}$$

Assume that all rods are of the same cross section and material; thus the bending stiffness, EI, is a constant. Let another constant, C, be the end-fixity coefficient for the single rod element. This parameter varies from one to four as the end fixity increases from pinned to clamped. If the rods are sufficiently slender, then the force in the filament causing fully elastic local buckling can be written as

$$P_{cr} = \frac{C\,\pi^2\,EI}{\Delta\ell^2}$$

or, from Eq. (1)

$$P_{cr} = \frac{C\,EI\,n^2}{r^2} \sin^2\beta \tag{2}$$

Assume that the loading is axisymmetric. Then two equilibrium equations can be written.

4

Let p_m and p_n be the external loads per unit surface area of the structure in the meridional and the normal directions, respectively, as shown in Figure 1. Also, let P be the compressive force in the filament. Now, examine the filament between two intersections with filaments of the other family. The corresponding surface area has the size $\dfrac{\pi r}{n}\dfrac{\Delta r}{\sin\alpha}$ and is traversed diagonally by the filament section, $\Delta\ell$. Equilibrium requires that in the direction of the z-axis

$$\Delta(P\cos\alpha\,\cos\beta) - p_m\frac{\pi r}{n}\frac{\Delta r}{\sin\alpha}\cos\alpha + p_n\frac{\pi r}{n}\frac{\Delta r}{\sin\alpha}\sin\alpha = 0$$

and in the radial direction

$$\Delta(P\sin\alpha\,\cos\beta) - P\sin\beta\,\frac{\Delta r\,\tan\beta}{\sin\alpha}\frac{1}{r} - p_m\frac{\pi r}{n}\frac{\Delta r}{\sin\alpha}\sin\alpha$$

$$- p_n\frac{\pi r}{n}\frac{\Delta r}{\sin\alpha}\cos\alpha = 0$$

Dividing by Δr and assuming that the filaments are sufficiently closely spaced that the difference quotient can be replaced by the derivatives, yields

$$\frac{d}{dr}(P\cos\alpha\,\cos\beta) - p_m\frac{\pi r}{n}\cot\alpha + p_n\frac{\pi r}{n} = 0$$

$$\frac{d}{dr}(P\sin\alpha\,\cos\beta) - P\frac{\sin\beta\,\tan\beta}{r\,\sin\alpha} - p_m\frac{\pi r}{n} - p_n\frac{\pi r}{n}\cot\alpha = 0$$

In order to find a more convenient second equilibrium equation, the first one is multiplied by $\cos\alpha\,\cos\beta$, the second one by $\sin\alpha\,\cos\beta$, and the results are summed:

$$\frac{dP}{dr} - \frac{\sin\beta}{r}\frac{d}{dr}(Pr\,\sin\beta) - p_m\frac{\pi r}{n}\frac{\cos\beta}{\sin\alpha} = 0$$

5

It is now postulated that at ultimate loading the compressive force, P , reaches the local fully elastic buckling load everywhere in the structure. Thus, P is replaced by P_{cr} from Eq. (2):

$$C\ EI\ n^2 \frac{d}{dr}\left(\frac{\sin^2\beta\ \cos\beta\ \cos\alpha}{r^2}\right) - p_m \frac{\pi}{n}\ r\ \cot\alpha + p_n \frac{\pi}{n}\ r = 0$$

$$C\ EI\ n^2 \left\{\frac{d}{dr}\left(\frac{\sin^2\beta}{r^2}\right) - \frac{\sin\beta}{r}\ \frac{d}{dr}\left(\frac{\sin^3\beta}{r}\right)\right\} - p_m \frac{\pi}{n}\ r\ \frac{\cos\beta}{\sin\alpha} = 0$$

Some manipulation yields a form convenient for subsequent use:

$$\left.\begin{aligned}
&\frac{d}{dr}\left(\frac{\sin^4\beta\ \cos^2\beta\ \cos^2\alpha}{r^4}\right) - \frac{2\pi\ p_m}{C\ EI\ n^3}\ \frac{\sin^2\beta\ \cos\beta\ \cos^2\alpha}{r\ \sin\alpha} \\[2mm]
&\qquad\qquad + \frac{2\pi\ p_n}{C\ EI\ n^3}\ \frac{\sin^2\beta\ \cos\beta\ \cos\alpha}{r} = 0 \\[3mm]
&\frac{d}{dr}\left(\frac{\sin^4\beta}{r^4}\right) - \frac{1}{r^2}\frac{d}{dr}\left(\frac{\sin^6\beta}{r^2}\right) - \frac{2\pi\ p_m}{C\ EI\ n^3}\ \frac{\sin^2\beta\ \cos\beta}{r\ \sin\alpha} = 0
\end{aligned}\right\}\quad (3)$$

These two equations allow the determination of the complete geometry of the structure in terms of the loading and the section properties of the rods.

Cylindrical Isostabiloids

A cylindrical case, such as is shown in Figure 5, can be construed as the limit of an annular type of axisymmetric structure with indefinitely increasing radius.

The differential equations for the geometry of cylindrical

6

isostabiloids can therefore be derived directly from the equations for axisymmetric structures, Eqs. (3), by substituting $(r_1 + x)$ for r and letting r_1 approach infinity. Consequently dr becomes dx, and the spacing of filaments

$$s = \frac{2\pi\, r_1}{n}$$

is introduced. The limiting process yields the basic equations for the cylindrical isostabiloid:

$$
\left.
\begin{aligned}
&\frac{d}{dx}\left(\sin^4\beta \,\cos^2\beta\, \cos^2\alpha\right) - P_m \frac{s^3}{4\pi^2\, C\, EI}\, \frac{\sin^2\beta\, \cos\beta\, \cos^2\alpha}{\sin\alpha} \\
&\qquad\qquad + P_n \frac{s^3}{4\pi^2\, C\, EI}\, \sin^2\beta\, \cos\beta\, \cos\alpha = 0 \\
&\frac{d}{dx}\left(\sin^4\beta\, \cos^2\beta\right) - P_m \frac{s^3}{4\pi^2\, C\, EI}\, \frac{\sin^2\beta\, \cos\beta}{\sin\alpha} = 0
\end{aligned}
\right\} \quad (4)
$$

7

GRAVITY LOADING

Consider the structure to be subject to its own weight with the direction of the gravitational force in the z-direction, and with g as the gravitational acceleration. Let ρ be the density of the rod material and A be the constant cross-sectional area. Then, the loads per unit surface area in the meridional and normal direction are, respectively,

$$p_m = \rho \, g \, A \, \frac{n}{\pi r} \, \frac{\cos\alpha}{\cos\beta}$$

$$p_n = - \, \rho \, g \, A \, \frac{n}{\pi r} \, \frac{\sin\alpha}{\cos\beta}$$

Eqs. (3) become

$$\frac{d}{dr} \left(\frac{\sin^4\beta \, \cos^2\beta \, \cos^2\alpha}{r^4} \right) - 2 \, \frac{\rho \, g \, A}{C \, EI \, n^2} \, \frac{\sin^2\beta \, \cot\alpha}{r^2} = 0$$

$$\frac{d}{dr} \left(\frac{\sin^4\beta}{r^4} \right) - \frac{1}{r^2} \frac{d}{dr} \left(\frac{\sin^6\beta}{r^2} \right) - 2 \, \frac{\rho \, g \, A}{C \, EI \, n^2} \, \frac{\sin^2\beta \, \cot\alpha}{r^2} = 0$$

Introducing nondimensional coordinates,

$$\left.
\begin{aligned}
R &= \left(\frac{\rho \, g \, A}{C \, EI \, n^2} \right)^{1/3} r \\[2em]
Z &= \left(\frac{\rho \, g \, A}{C \, EI \, n^2} \right)^{1/3} z
\end{aligned}
\right\} \tag{5}$$

and defining a variable

$$h = \sin^2\beta$$

yields the differential equations for the geometry of a gravity-loaded axisymmetric isostabiloid

$$\frac{d}{dR}\left(\frac{h^2(1-h)\ \cos^2\alpha}{R^4}\right)- 2\ \cot\alpha\ \frac{h}{R^2} = 0$$

$$\frac{d}{dR}\left(\frac{h^2}{R^4}\right) - \frac{1}{R^2}\frac{d}{dR}\left(\frac{h^3}{R^2}\right) - 2\ \cot\alpha\ \frac{h}{R^2} = 0 \tag{6}$$

A parallel procedure can be applied to the cylindrical configuration. If the lengthwise coordinate is defined as y, the appropriate nondimensionalization is

$$\overline{X} = \frac{\rho\ g\ A\ s^2}{4\pi^2\ C\ EI}\ x$$

$$\overline{Y} = \frac{\rho\ g\ A\ s^2}{4\pi^2\ C\ EI}\ y \tag{7}$$

$$\overline{Z} = \frac{\rho\ g\ A\ s^2}{4\pi^2\ C\ EI}\ z$$

The resulting differential equations for the gravity-loaded cylincrical isostabiloid are:

$$\frac{d}{d\overline{X}}\ [h^2\ (1-h)\ \cos^2\alpha] - 2h\ \cot\alpha = 0$$

$$\frac{d}{d\overline{X}}\ [h^2\ (1-h)] - 2h\ \cot\alpha = 0 \tag{8}$$

9

Domes

Equations (6) have to be solved numerically. Because closed dome-shaped isostabiloids are of most interest, efforts are concentrated on this type of solution. The equations are clearly singular at $R = 0$, and careful attention must be given to the behavior of the solution at this point. The differential equation of the meridian is

$$\frac{dZ}{dR} = \cot\alpha$$

If domes exist, that is, if $\alpha = 90°$ for $R = 0$, it must be possible to develop the meridian, Z, and consequently $\cot\alpha$, as well as h in power series in R:

$$\cot\alpha = \sum_{i=0}^{\infty} \lambda_i R^i$$

$$h = \sum_{j=0}^{\infty} h_j R^j$$

By applying the differential equations (6) to these series it can be shown that there is a unique solution

$$\cot\alpha = \lambda_1 R + O(R^3)$$

$$h = h_2 R^2 + O(R^4)$$

and that
$$\lambda_1 = \frac{1}{h_2}$$

The meridional shape near the center, therefore, becomes

$$Z = Z_o + \frac{\lambda_1}{2} R^2$$

Thus λ_1 represents the nondimensional curvature of the meridian at the apex. Call it k.

For the purpose of numerical integration the differential equations (6) are rewritten as

$$\frac{d\alpha}{dR} = \frac{h^2 \cot\alpha - R^3}{Rh(1-h)}$$

$$\frac{dh}{dR} = \frac{h(2-h) + R^3 \cot\alpha}{R(1 - \frac{3}{2} h)}$$

and the first term approximations

$$\cot\alpha = k\,R$$
$$h = \frac{1}{k} R^2$$
$$z = z_o + \frac{k}{2} R^2$$

are used to start the process.

In the course of integration the independent variable is switched from R to h in order to avoid a division by zero when h reaches the value of 2/3. This value is significant because the meridian ends there $\left(\frac{dR}{dh} = \frac{dZ}{dh} = 0\right)$. Thus, on a closed-dome axisymmetric isostabiloid, the filament angle, β, can vary only between 0° and 54.74°.

Because of the closed-dome specification, the filament path, $\beta(R)$, and the meridional shape, $\alpha(R)$, consequently also $Z(R)$ and the height-to-semispan ratio, z_o/r_o, are completely defined if the nondimensional curvature at the apex, k, and the termination of the integration, R_o, α_o, or β_o, are selected.

For example, Figure 2 shows side and top views of a dome-shaped isostabiloid, specified by the curvature, $k = 2$, and

11

the filament angle at the rim, $\beta_o = 54.74°$.

The nondimensional curvature at the apex, k, is an independent design parameter. It is needed for the numerical evaluation, but it provides little information about the structural configuration. For the selection of a particular dome, therefore, a more practical design parameter, the height-to-semispan ratio, z_o/r_o, is plotted in Figure 3 versus the integration limit, R_o with k as parameter. In addition, the values of α_o and β_o corresponding to each combination of R_o and k are indicated by lines of constant value. Therefore Figure 3 is a design chart for dome-shaped isostabiloid configurations because now any desired combination of the parameters, α_o, β_o, R_o, z_o/r_o, and k, can be picked to select a unique configuration.

As an example, domes with a height-to-semispan ratio, z_o/r_o = 1, 2, and 3, and $\beta_o = 54.74°$ are seen to be characterized by k-values of approximately 3, 6, and 10, respectively. Their meridians have been computed and are shown in a normalized form in Figure 4.

Tunnels

For the cylindrical configuration, attention is directed to singly-connected tunnel-type shapes. Equations (8) can be re-written as

$$\frac{d}{d\overline{X}} \left(h^2 (1-h) \sin^2\alpha \right) = 0$$

$$\frac{d}{d\overline{X}} \left(h^2 (1-h) \right) - 2h \cot\alpha = 0$$

The first differential equation can be integrated to yield

$$\sin^2\alpha = \frac{b^2 (1-b)}{h^2 (1-h)}$$

12

where $b = \sin^2\beta_a$ at the apex, where $\alpha = \pi/2$. Substitution into the second equation yields

$$\frac{d}{d\overline{X}}\left(h^2\,(1-h)\right) \mp 2h\sqrt{\frac{h^2\,(1-h)}{b^2\,(1-b)} - 1} = 0$$

or

$$d\overline{X} = \pm\,\frac{b\sqrt{1-b}\,\left(1-\frac{3}{2}h\right)}{\sqrt{h^2\,(1-h) - b^2\,(1-b)}}\,dh$$

If the integration starts at $h = b$, tunnels closed at the apex are produced because the $\pm$ sign in the differential equation implies a symmetry with respect to the origin of the $\overline{X}$-coordinate.

The cross-sectional shape of the cylinder and the lengthwise pattern of the filaments are determined by the two equations

$$d\overline{Z} = \cot\alpha\ d\overline{X} = \pm\,\left(1 - \frac{3}{2}\,h\right)\,dh$$

and

$$d\overline{Y} = \frac{\tan\beta}{\sin\alpha}\ d\overline{X} = \pm\,\frac{h^{3/2}\,\left(1 - \frac{3}{2}\,h\right)}{\sqrt{h^2(1-h) - b^2(1-b)}}\,dh$$

The polynomial under the radical in the denominator of the formulas for $d\overline{X}$ and $d\overline{Y}$ can be written as

$$h^2(1-h) - b^2(1-b) = (a-h)\,(h-b)\,(h-c)$$

where

$$a = \frac{1-b}{2}\,\left(1 + \sqrt{1 + \frac{4b}{1-b}}\right)$$

13

and
$$c = \frac{1-b}{2} \left(1 - \sqrt{1 + \frac{4b}{1-b}} \right)$$

Now the coordinates, $\overline{X}$ and $\overline{Y}$, can be written in terms of ellip-
tic integrals

$$\overline{X} = b\sqrt{1-b} \int_b^h \frac{(1 - \frac{3}{2} h)}{\sqrt{(a-h)(h-b)(h-c)}} \, dh$$

$$\overline{Y} = \int_b^h \frac{h^{3/2}(1 - \frac{3}{2} h)}{\sqrt{(a-h)(h-b)(h-c)}} \, dh$$

while
$$\overline{Z} = \int_b^h (1 - \frac{3}{2} h) \, dh$$

Note that a and b are exchangeable, and that further-
more a = b for b = 2/3 . But this, too, is the point where $\overline{X}$
and $\overline{Z}$ reverse their directions in the integration. Therefore,
again, at h = 2/3 the rim is reached. For values of b
smaller than 2/3 , the filament angle, β , increases from its
value at the apex, β_a , to 54.74°, while for b larger than 2/3,
β decreases from the apex to the rim.

An investigation of the nondimensional curvature at the
apex, k , shows that

$$k = \frac{d^2 \overline{Z}}{d\overline{X}^2} = \frac{d(\cot\alpha)}{dh} \frac{dh}{d\overline{X}} = \frac{1}{b(1-b)}$$

and therefore can never be smaller than 4.

14

As in the dome structure, the geometry of the tunnel is determined by specifying the behavior at the apex (it is β_a, b, or k whichever form is preferred) and the end of the intergration (α_o, β_o, or $\overline{X}_o$). For example, Figure 5 shows an isometric projection of a cylindrical isostabiloid specified by the two values of the filament angle, β: 30° at the apex (equivalent to b = 0.25 or k = 5.333) and 54.74° at the rim.

Figures 6 and 7 present the design charts for the configuration of cylindrical isostabiloids, with filament angles at the apex, β_a, smaller than 54.74° in Figure 6 and larger than 54.74° in Figure 7. Again, from this chart the design parameters are chosen which pertain to cross-sections of tunnels with a height-to-semispan ratio, z_o/x_o, of 1, 2, and 3, shown in Figure 8.

MASS OF THE GRAVITY-LOADED STRUCTURES

Because gravity is the only external load, the mass of the structure can be determined from the forces exerted upon the edge support. Each filament contributes to the total vertical load the amount, $P_{cr} \cos\alpha_o \cos\beta_o$, where P_{cr} is defined by Eq. (2). Thus the average structural mass per unit planform area, m, is, for domes,

$$m = \frac{2n\, P_{cr}\, \cos\alpha_o\, \cos\beta_o}{g\, \pi\, r_o^2}$$

and for tunnels,

$$m = \frac{2\, P_{cr}\, \cos\alpha_o\, \cos\beta_o}{s\, g\, x_o}$$

Let the moment of inertia of the individual structural member be related to its area by the formula

$$I = K_f\, A^2$$

where K_f is a shape factor. Also replace P_{cr} by Eq. (2), then for domes,

$$m = \frac{2n^3\, C\, E\, K_f\, A^2}{g\, \pi\, r_o^4}\, \sin^2\beta_o\, \cos\beta_o\, \cos\alpha_o \qquad (9)$$

and for tunnels,

$$m = \frac{8\pi^2\, C\, E\, K_f\, A^2}{g\, s^3\, x_o}\, \sin^2\beta_o\, \cos\beta_o\, \cos\alpha_o \qquad (10)$$

16

Now, from Eq. (5), for domes,

$$A = \frac{\rho \, g}{C \, E \, K_f \, n^2} \left(\frac{r_o}{R_o}\right)^3 \tag{11}$$

Also, from Eq. (7), for tunnels,

$$A = \frac{\rho \, g \, s^2}{4\pi^2 \, C \, E \, K_f} \, \frac{x_o}{\overline{X}_o} \tag{12}$$

If these expressions for A are substituted into the appropriate formulas for mass, and the spacing at the rim of the dome

$$s_o = \frac{2\pi \, r_o}{n}$$

is introduced, the following results are obtained.

For domes,

$$m = \frac{\rho^2 \, g \, s_o \, r_o}{\pi^2 \, C \, E \, K_f} \, f_D \tag{13}$$

and for tunnels,

$$m = \frac{\rho^2 \, g \, s \, x_o}{\pi^2 \, C \, E \, K_f} \, f_T \tag{14}$$

The functions, f_D and f_T , are expressed in terms related to the structural configuration alone and, therfore, are called weight form factors:

17

$$f_D = \frac{\sin^2\beta_o \, \cos\beta_o \, \cos\alpha_o}{R_o^6}$$

$$f_T = \frac{\sin^2\beta_o \, \cos\beta_o \, \cos\alpha_o}{2\bar{X}_o^2}$$

They are plotted in Figure 9 versus the height-to-semispan ratio z_o/r_o or z_o/x_o , with the nondimensional radius of the dome, R_o , and the nondimensional semispan of the tunnel, $\bar{X}_o$ respectively, as parameter (full lines). For easier interpretation, lines of constant k-values are also indicated (dashed) in the two graphs.

It has been found above that for constant k-values the filament angle at the rim, β_o , increases or decreases steadily with growing R_o- and $\bar{X}_o$- values. Consequently, Figure 9 shows that for constant values of k the weight form factors of gravity-loaded axisymmetric isostabiloids become a minimum when β_o reaches its maximum possible value of 54.74°. The global minimum of the weight form factor, $f_D = 6.07$, is achieved for an iso-stabiloid dome with a height-to-semispan ratio z_o/r_o of approximately 0.53. A view of this "minimum weight" isostabiloid is shown in Figure 10.

In the case of cylindrical structures, only values of f_T for β_a smaller than 54.74° are shown because for larger values the factor, f_T , is considerably larger. Note that unlike f_D , the minimum of f_T for constant k-values is not always coupled with the largest possible filament angle at the rim. The global minimum, $f_{T_{min}} = 3.6$, however, does belong to a configuration with an angle, β_o , of 54.74° and a z_o/x_o of 0.6.

Examination of Eqs. (13) and (14) shows that the operative parameter for material efficiency is E/ρ^2 .

Of particular interest is the fact that the structural mass is proportional to the spacing of the filaments. This implies a weightwise advantage of finely textured structures. However, a limit is provided by the lowest order failure mode of general instability.

DESIGN LIMITATIONS

Recall the intrinsic assumptions of the foregoing analytical design procedure, i.e.,

- The instability failure takes place in the fully linear, elastic range, and

- The instability failure mode of the structure which characterizes the design consists of nodes at each filament intersection.

Hence, for the procedure to yield a valid design it is necessary that

- The stress at ultimate loading must remain at or below the proportional limit of the structural material, and at or below the local crippling stress of the structural section employed, and

- No "general" instability failure modes occur at loading levels below that which corresponds to the postulated design failure mode.

The two design limitations resulting from these requirements will be discussed separately below.

Stress Limits

The stress limitation of isostabiloid design is subject to rigorous analysis. It can be shown that the maximum stress is reached at the rim. Using Eqs. (2) and (11), and (2) and (12) yields for domes:

$$\sigma_{o_D} = \rho \, g \, r_o \, \overline{f}_D \tag{15}$$

and for tunnels

$$\sigma_{o_T} = \rho \, g \, x_o \, \overline{f}_T \tag{16}$$

19

with the non-dimensional parameters

$$\overline{f}_D = \frac{\sin^2 \beta_o}{R_o^3}$$

$$\overline{f}_T = \frac{\sin^2 \beta_o}{\overline{X}_o}$$

The functions $\overline{f}_D$ and $\overline{f}_T$ are stress form factors because they depend, again, on the configuration alone. They are plotted in Figure 11. Note that $\overline{f}_T$ is presented only for values of β_a smaller than 54.74° because, as in the case of the weight form factor, $\overline{f}_T$ for β_a larger than 54.74° assumes considerably higher values.

No distinct global minimum for $\overline{f}_D$ and $\overline{f}_T$ appears in Figure 11. Indeed, a closer examination shows that for decreasing parameter values of R_o or $\overline{X}_o$, as well as for increasing k-values the corresponding minima of $\overline{f}$ approach a value of 1.5 at z_o/r_o or z_o/x_o equal to 0.75. But, as it may be checked in the design charts, Figures 3 and 6, in the same process the filament angle at the rim, β_o, becomes very small and the corresponding isostabiloids theoretically degenerate into domes with plane, non-intersecting radial members and into tunnels consisting of plane arches perpendicular to the tunnel axis. In addition, Figure 9 shows tremendously increasing weight form factors for the corresponding configurations. Consequently, in cases where the stress limit really might be reached, a compromise between weight and stress consideration has to be sought.

A look at the stress equations provides an idea when the stress becomes pertinent: the semispan of isostabiloid structures will be stress limited at

$$r_{o_{max}} = \frac{\sigma_{max}}{\rho g} \frac{1}{\bar{f}_D} \tag{17}$$

and

$$x_{o_{max}} = \frac{\sigma_{max}}{\rho g} \frac{1}{\bar{f}_T} \tag{18}$$

Note that $\frac{\sigma_{max}}{\rho g}$ is the specific working stress, and that $1/\bar{f}$ assumes a value of 2/3 or less. Hence, the largest, stress limited structure will have a span of approximately 4/3 times the specific working stress.

For example, an earth based aluminum construction (ρg_{earth} = 0.1 lb/in.^{3}) operating at a maximum safe stress level of 10,000 psi would yield a span of 130,000 in. or approximately two miles! On the moon surface (ρg_{moon} = 0.0165 lb/in.^{3}) a similar structure would be stress limited at a span of almost 13 miles. Even with only half the values of $1/\bar{f}$, assuring weight form factors close to the global minimum, the stress limited structures assume enormous proportions.

General Instability Limits

For the cylindrical structure, it is evident that the lowest instability mode will tend to have nodes only at the foundations and at the apex. Thus, the only "isostabiloid" would be the extremely degenerate case where the filaments do not intersect at locations other than at the apex; auxiliary braces will be required to prevent premature general instability failure. Since the dead weight loading associated with these braces has not been considered in the analysis, the design procedure will at best yield a first approximation to the desired optimum structure.

For domes, the situation is more complex. Let $\bar{n}$ be the number of rod sections contained in each filament between apex and rim. Then for a structure with $2n$ filaments, the number of unrestrained filament intersections is

$$N = n \, (\overline{n} - 1) + 1$$

The elastic properties of the structure thus can be expressed by a stiffness matrix of order 3N or 6N , depending on the nature of rotational constraints at the intersections. Eigenvector extraction yields the buckling modes for the corresponding 3N (or 6N) critical loads. The associated computational problem for any but the simplest structures is enormous and a rigorous parametric treatment is beyond the scope of this study. However, one simpler way to determine approximately the conditions under which general failure occurs is explored in the appendix.

APPLICATIONS

Two sample designs are given to demonstrate the applications of the isostabiloid design procedure.

Consider earth based isostabiloid domes. One dome shall have the optimal proportions for minimum structural weight, shown in Figure 10, the other shall be a design characterized by a low stress form factor and the same height-to-semispan ratio as the minimum weight dome. Its configuration is shown in Figure 12. Both domes shall be constructed from aluminum alloy tubing. An ultimate design factor of 4 shall be applied to the gravity loading, and the design shall be balanced to produce local crippling of the tubing at the materials proportional limit, σ_p, in the most severely stressed rim members. At the same limit stress, Euler buckling of all members is to occur. The size and detail construction of domes meeting these conditions shall be determined.

The pertinent non-dimensional parameters are tabulated below:

TABLE I

	Minimum Weight Configuration	Low-Stress-Factor Configuration
R_o	0.59	0.39
Z_o	0.31	0.20
β_o	54.7°	18.3°
α_o	47.1°	42.3°
f_D	6.07	20.2
$\bar{f}_D$	3.21	1.68

23

The materials properties are assumed to be

$$E = 10^7 \text{ psi}$$

$$\rho g_E = 0.101 \text{ lb/in.}^3$$

$$\sigma_p = 40,000 \text{ psi}$$

To meet the required design factor of 4, the maximum permissible working stress under simple gravity load is

$$\sigma_o = 10,000 \text{ psi}$$

The size of the dome is now determined by Eq. (17)

$$r_o = \frac{\sigma_o}{\rho g_E \, \overline{f}_D}$$

This yields

$r_o = 2,570 \text{ ft}$ for the minimum weight configuration, and

$r_o = 4,890 \text{ ft}$ for the low-stress-factor configuration.

The diameter, D , and wall thickness, t , of the tubing is chosen such that local crippling of the wall will occur at the proportional limit. Hence, from Reference 3:

$$\sigma_{cr} = \sigma_p = 0.4 \, E \, t/D = 40,000 \text{ psi}$$

or $t/D = 0.01$

and $K_f = \dfrac{I}{A^2} = \dfrac{D}{8\pi t} = 3.98$

24

The structure shall be built such that its members will buckle at a load equal to 4 times that which is produced by its own gravity. Equation (5) can be rewritten to yield the diameter of the structural tubing which will satisfy this condition:

$$\frac{D^2}{8} = I/A = \frac{r_o^3}{R_o^3} \frac{4(\rho g)}{CEn^2}$$

and, assuming $C = 1$:

$$D = \frac{6750}{n} \quad \text{for the minimum weight configuration, and}$$

$$D = \frac{33600}{n} \quad \text{for the low-stress-factor configuration.}$$

The weight of the structure is found from Eq. (13), which can be rewritten, by substituting

$$g = 4 \, g_E \, , \quad \text{and} \quad s_o = \frac{2\pi \, r_o}{n}$$

which yields:

$$W = mg_E \, r_o^2 \pi = \frac{8 \, r_o^4 \, (\rho g_E)^2 f_D}{n \, C \, E \, K_f}$$

or

$$W = \frac{1.13 \times 10^{10}}{n} \text{ lb} \quad \text{for the minimum weight configuration, and}$$

$$W = \frac{47.9 \times 10^{10}}{n} \text{ lb} \quad \text{for the low-stress-factor configuration.}$$

Table II and III below summarize the properties of isostabiloid domes for various values of n ,

TABLE II

MINIMUM WEIGHT CONFIGURATION

n	36	72	100	250	500	1000
D (in.)	187.5	93.75	67.5	27	13.5	6.75
t (in.)	1.875	0.9375	0.675	0.27	0.135	0.0675
W (10^6 lb)	313.5	157	113	45.2	22.6	11.3

TABLE III

LOW-STRESS-FACTOR CONFIGURATION

n	24	36	60	100	180	360	720
D (in.)	1400	937.5	560	336	187	93.75	46.9
t (in.)	14	9.375	5.6	3.36	1.87	0.9375	0.47
W (10^9 lb)	20	13.3	7.98	4.79	2.66	1.33	0.665

Moon Structure:

Future bases located on the surface of the moon will require shelters for personnel, material and equipment. An isostabiloid dome may be employed as a scaffold in the initial phase of the construction of such shelters. Since the structure will be transported from the surface of the earth, minimum weight and storage volume will be required.

As an example of such a structure, consider a "minimum weight" isostabiloid dome with a diameter of 333 feet (r_o = 2000") and apex height of 88 feet. It is to be designed with a load factor of 3 for operation in the moons gravitational field of 1/6 g_E, and the dome is to be made from flattenable and coilable "Sintes-Tubes" (Ref. 5).

The cross section of this type of structural member is shown in Figure 13. As material of construction 17-7 PH Stainless Steel is selected with the following properties:

$$E = 28 \times 10^6 \text{ psi}, \quad (\rho g_E) = 0.28 \text{ lb/in.}^3, \quad \sigma_y = 180,000 \text{ psi}$$

The maximum working stress at the rim is given by Eq. (15)

$$\sigma_o = r_o \frac{1}{6} (\rho g_E) \overline{f}_D = 300 \text{ psi}$$

This structure will obviously not be stress limited.

The wall thickness/convolute diameter ratio of the structural tubes, t/d, is determined by the condition for flattening: Allowing a maximum strain of .33% during the flattening process requires $d/t = 300$ and yields a stiffness form factor $K_f = 15.6$. The (earth) weight of the structure is derived from Eq. (13)

$$W_E = r_o^2 \pi mg_E = \frac{r_o^4 (\rho g_E)^2}{n C E K_f} = \frac{4360}{n} \text{ lb}$$

and the cross sectional dimension of the tubing (see Fig. 13) become

$$d_1 = \frac{49.8}{n} \text{ in.} \qquad d_2 = \frac{45.3}{n} \text{ in.} \qquad t = \frac{0.0798}{n} \text{ in.}$$

Reasonable structural sections are obtained by choosing
n = 72 . The structural properties and dimensions for this
design are given in Table IV below:

TABLE IV

333 FT DIAMETER MOON DOME STRUCTURE, n = 72

Design Factor	3
Weight (lbm)	60.5
d_1 (in.)	0.69
d_2 (in.)	0.63
t (mils)	1.1

CONCLUDING REMARKS

A mathematical formulation suitable for analytical design of structural networks with uniform local instability margins has yielded solutions for specific, idealized cases of simple, two-family "axisymmetric" and "cylindrical" networks. Such structural configurations may form the basis for the design lay-out of practical structures. Not considered were the effects of unavoidable local and general imperfections upon the optimal choice of design configurations, and the effect of multiple loading conditions. In addition, only one type of loading was treated in detail, and the influence of general instability phenomena was only shortly discussed. A fertile field for further theoretical and experimental studies is indicated.

Figure 1. Isostabiloids – Geometry and Forces of an Element

Figure 2. Typical Gravity-Loaded Axisymmetric Isostabiloid
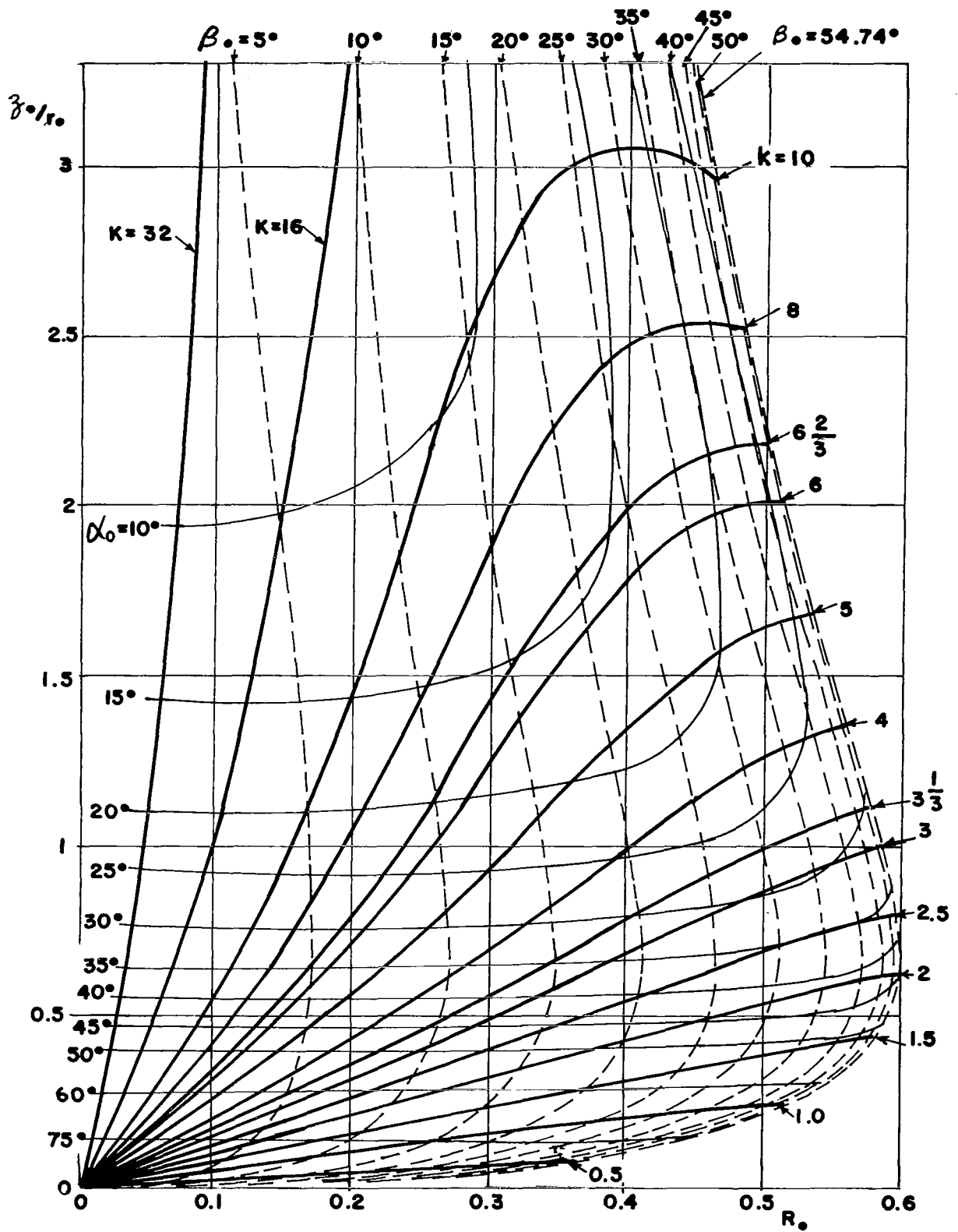Top and Side Views

31

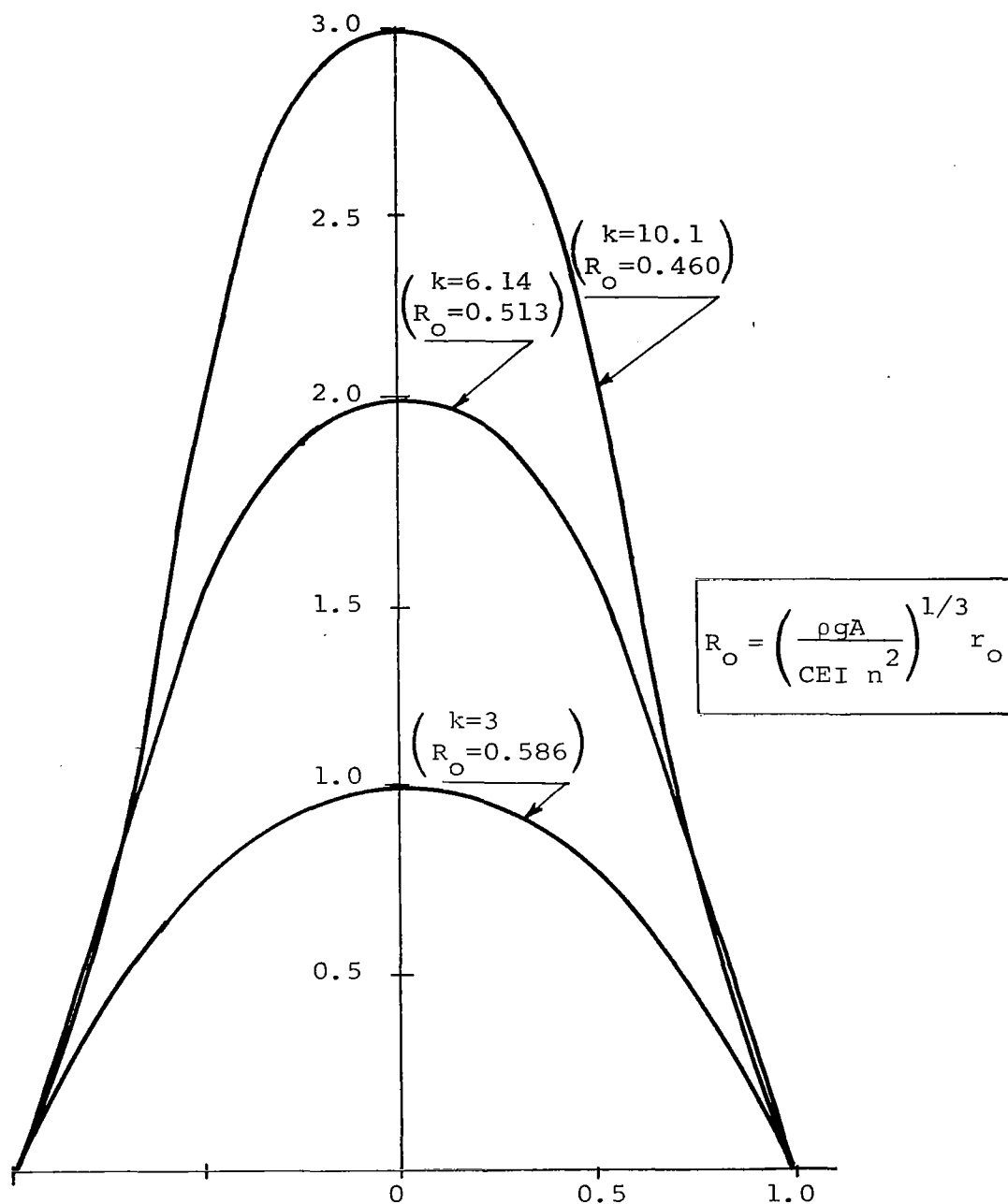Figure 3. Configuration Design Chart for Dome-Shaped Isostabiloids

$$R_O = \left(\frac{\rho g A}{CEI_n^2} \right)^{1/3} r_O$$

$\left(\begin{array}{c} k=6.14 \\ R_O=0.513 \end{array} \right)$

$\left(\begin{array}{c} k=10.1 \\ R_O=0.460 \end{array} \right)$

$\left(\begin{array}{c} k=3 \\ R_O=0.586 \end{array} \right)$

Figure 4. Gravity-Loaded Axisymmetric Isostabiloids Meridians for $\beta_O = 54.74°$; $z_O/r_O = 1$, 2, and 3

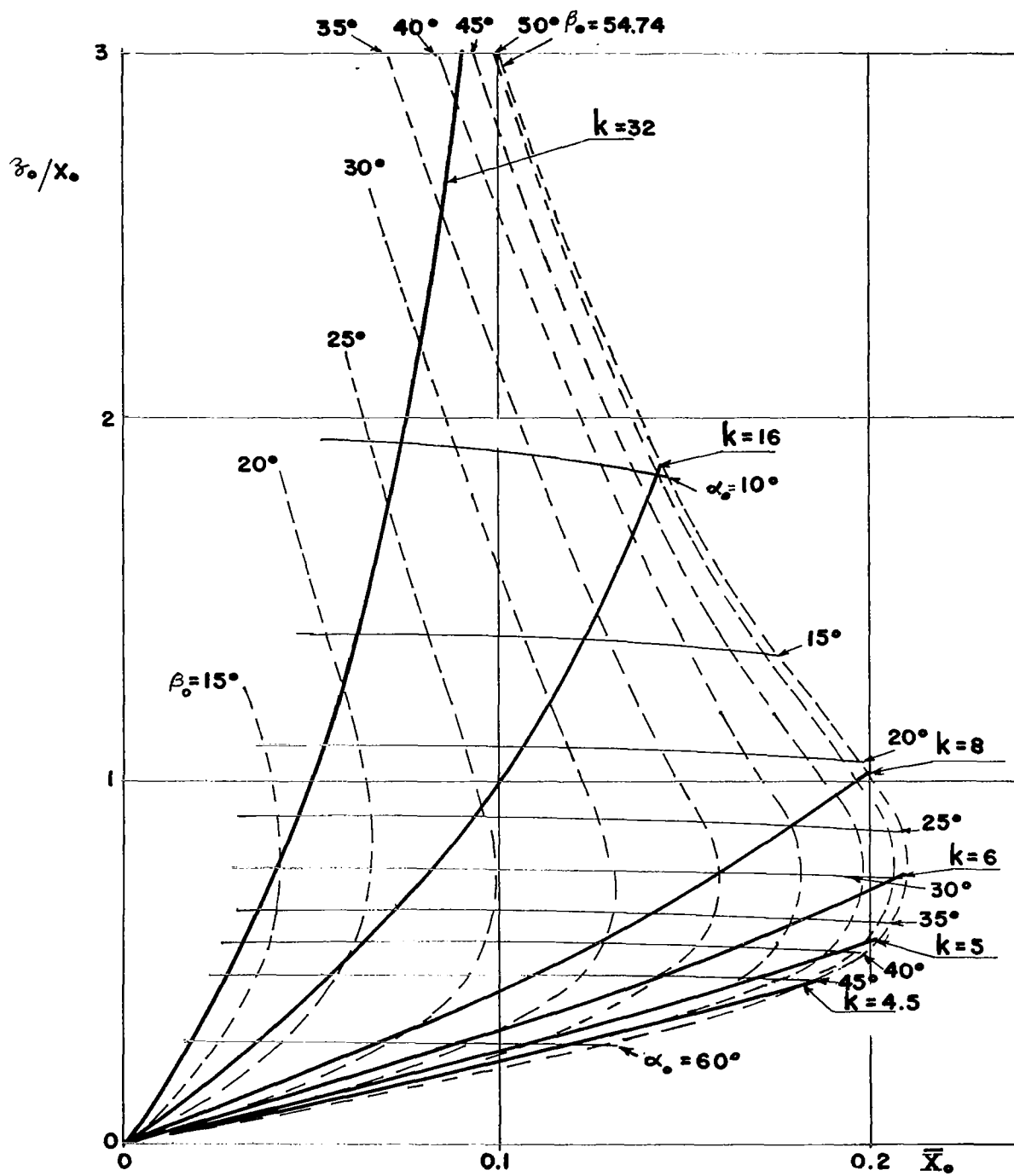Figure 5.   Cylindrical Isostabiloid, Gravity-Loaded $\beta_a = 30°$, $\beta_o = 54.74°$

Figure 6.   Configuration Design Chart for Tunnel-Shaped
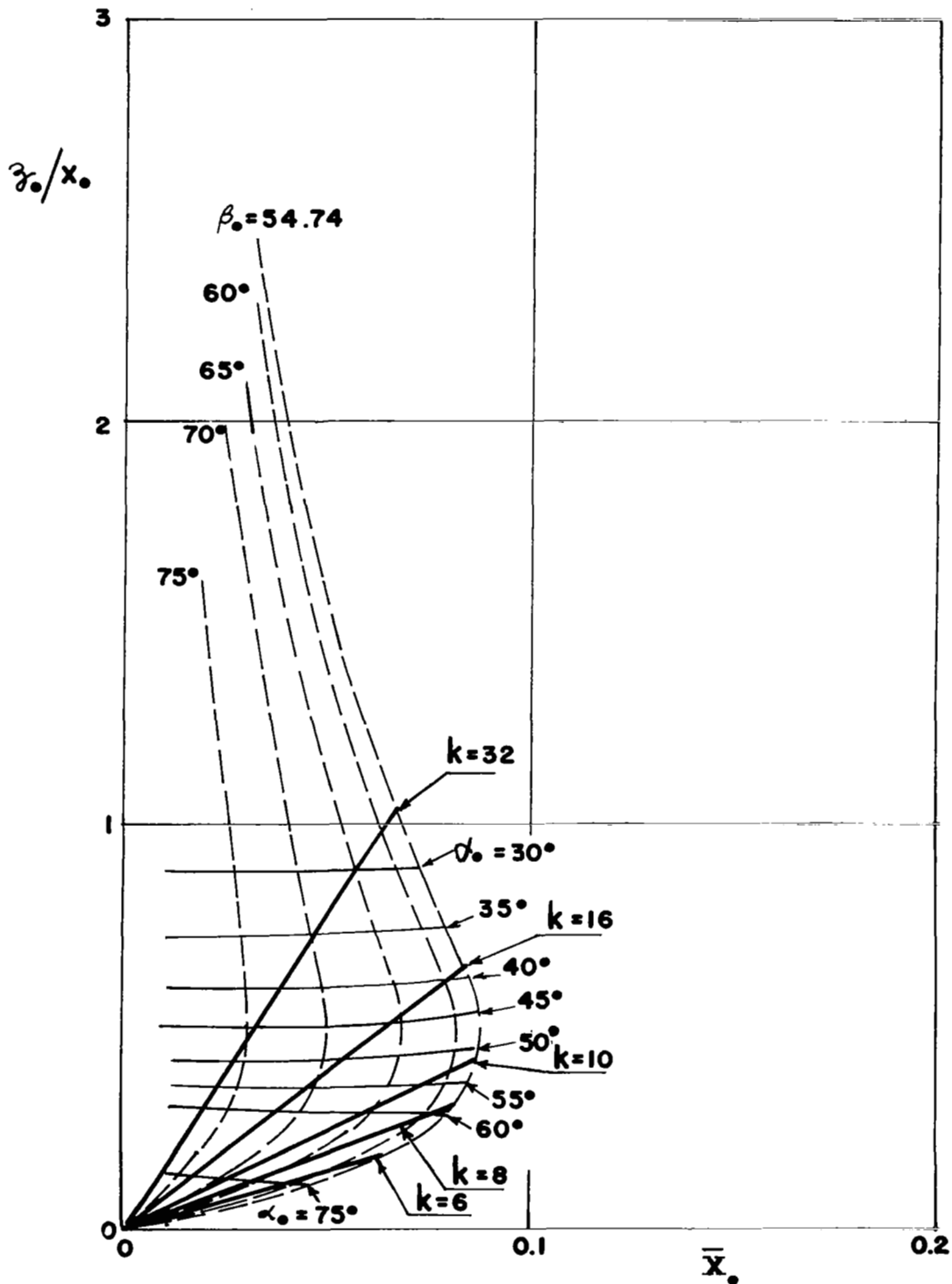Isostabiloids
(β_a < 54.74° or b < 2/3)

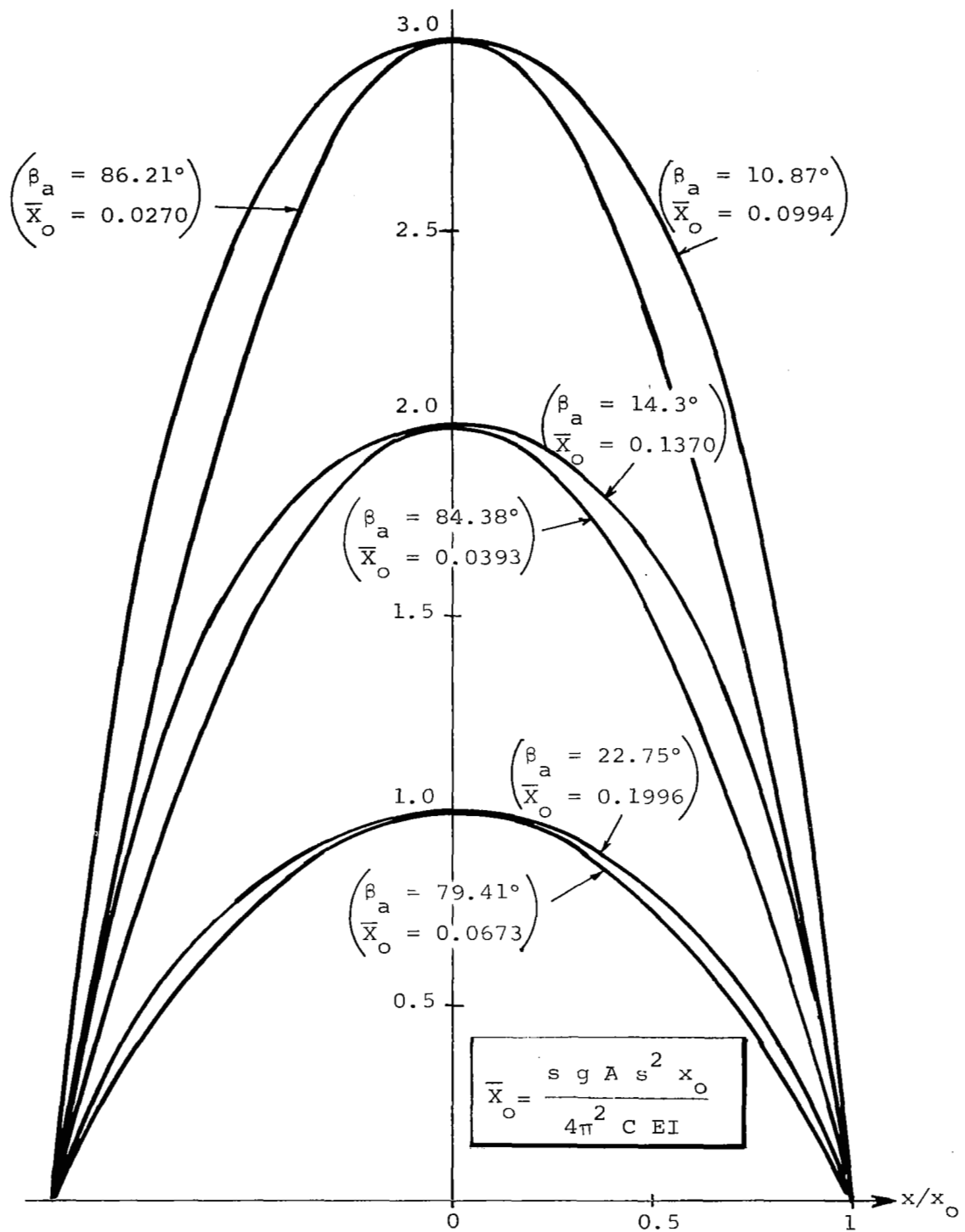Figure 7. Configuration Design Chart for Tunnel-
Shaped Isostabiloids
$(\beta_a > 54.74°$ or $b > 2/3)$

Figure 8. Gravity-Loaded Cylindrical Isostabiloids Cross-Sections for $\beta_o = 54.74°$; $z_o/x_o = 1$, 2, and 3

The figure contains the following labels:

$\left(\begin{array}{l}\beta_a = 86.21° \\ \overline{X}_o = 0.0270\end{array}\right)$

$\left(\begin{array}{l}\beta_a = 10.87° \\ \overline{X}_o = 0.0994\end{array}\right)$

$\left(\begin{array}{l}\beta_a = 14.3° \\ \overline{X}_o = 0.1370\end{array}\right)$

$\left(\begin{array}{l}\beta_a = 84.38° \\ \overline{X}_o = 0.0393\end{array}\right)$

$\left(\begin{array}{l}\beta_a = 22.75° \\ \overline{X}_o = 0.1996\end{array}\right)$

$\left(\begin{array}{l}\beta_a = 79.41° \\ \overline{X}_o = 0.0673\end{array}\right)$

$$\overline{X}_o = \frac{s\,g\,A\,s^2\,x_o}{4\pi^2\,C\,EI}$$
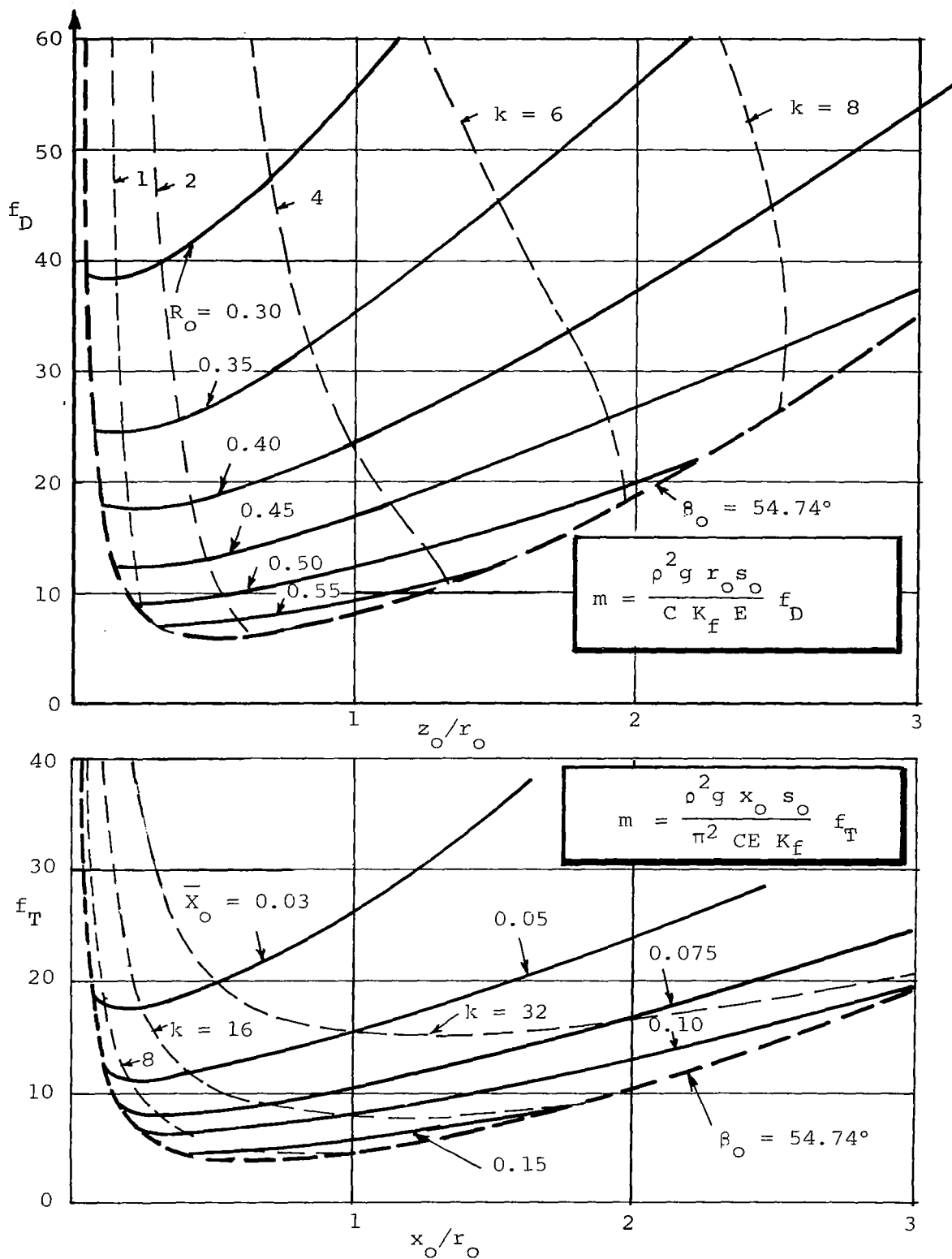
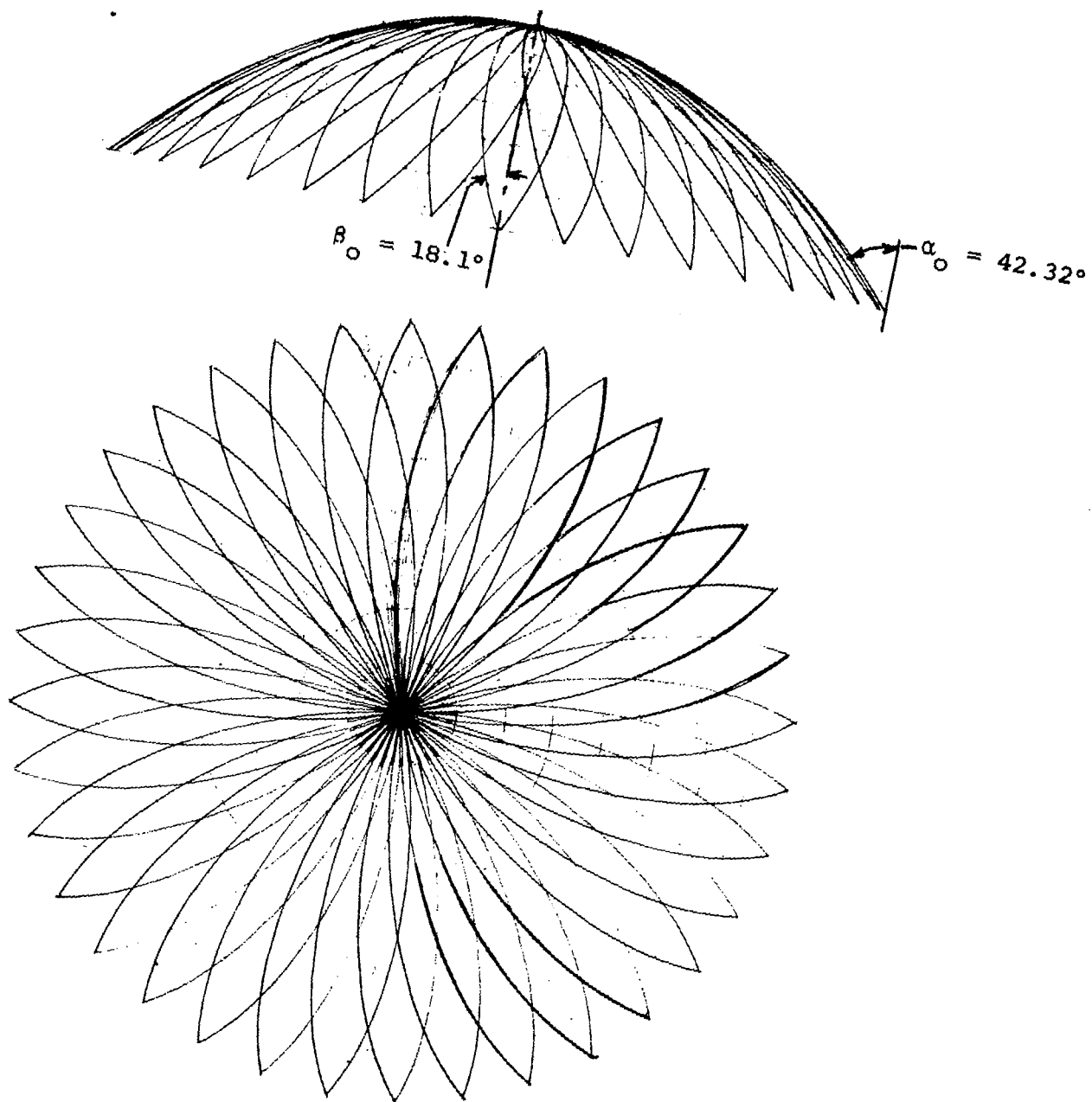Figure 9. Axisymmetric and Cylindrical Isostabiloids
Weight per Covered Area

Figure 10. Axisymmetric Isostabiloid: Side and Top Views
Gravity-Loaded, Global Minimum Weight Configuration
$k = 1.726$, $\beta_o = 54.74°$, $(R_o = 0.5922$, $z_o/r_o = 0.5283)$
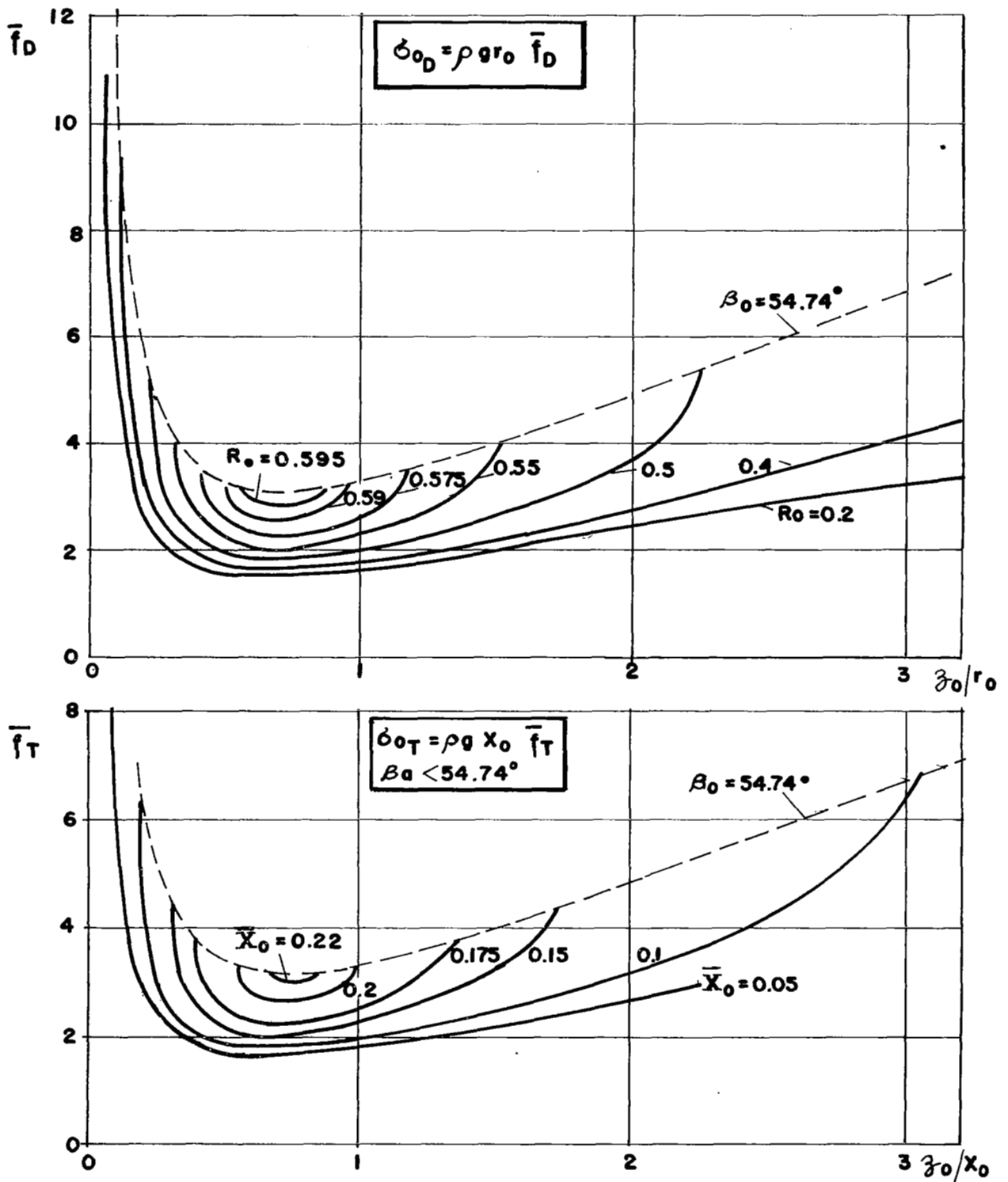
$\beta_o = 18.1°$

$\alpha_o = 42.32°$

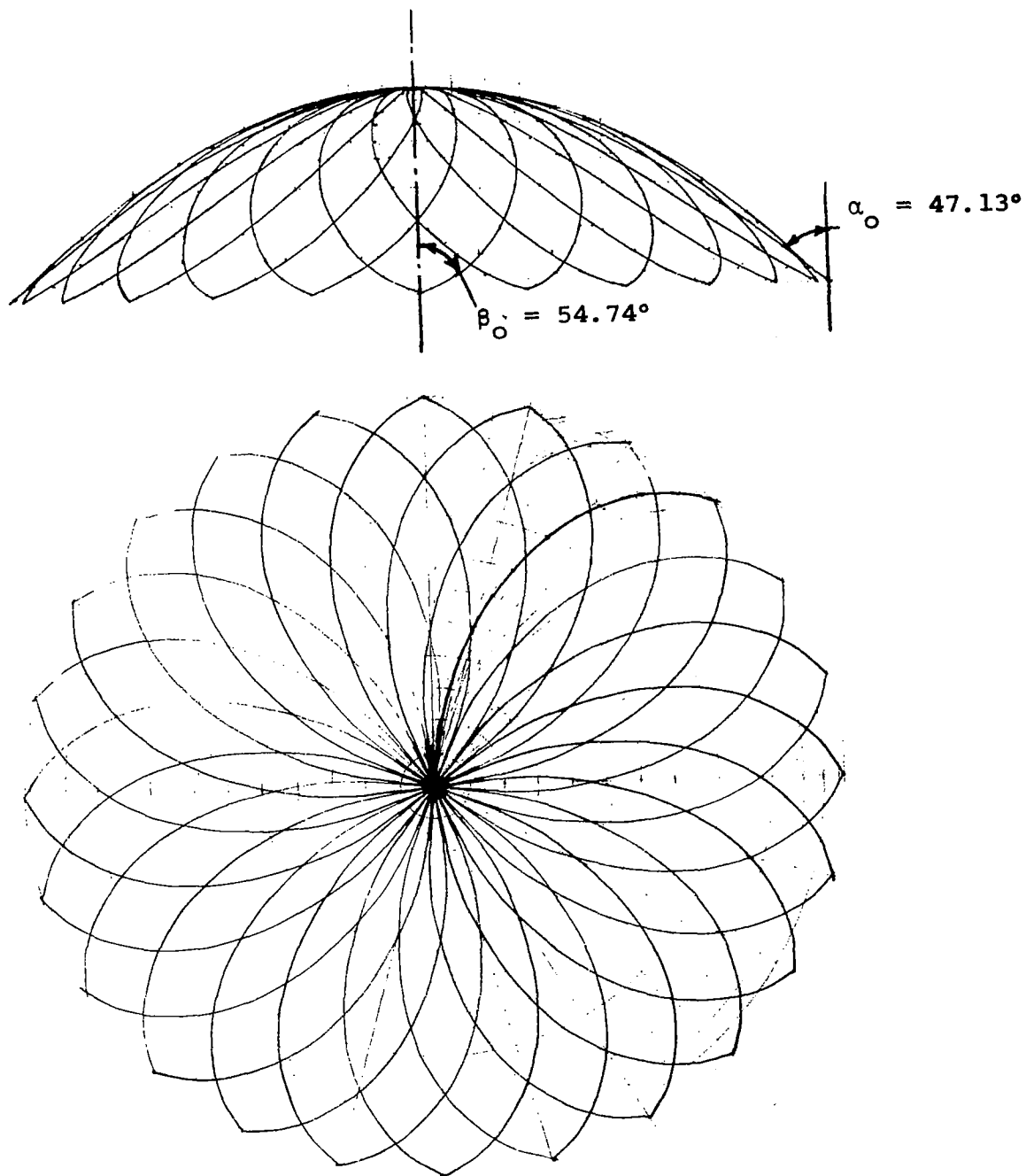Figure 11. Axisymmetric and Cylindrical Isostabiloids
Rim-Stress Form Factor

Figure 12. Axisymmetric Isostabiloid: Side and Top Views of Low-Stress Form Factor Configuration for $z_o/r_o = 0.5283$ $k = 2.475$, $\beta_o = 18.1°$ ($R_o = 0.3875$)
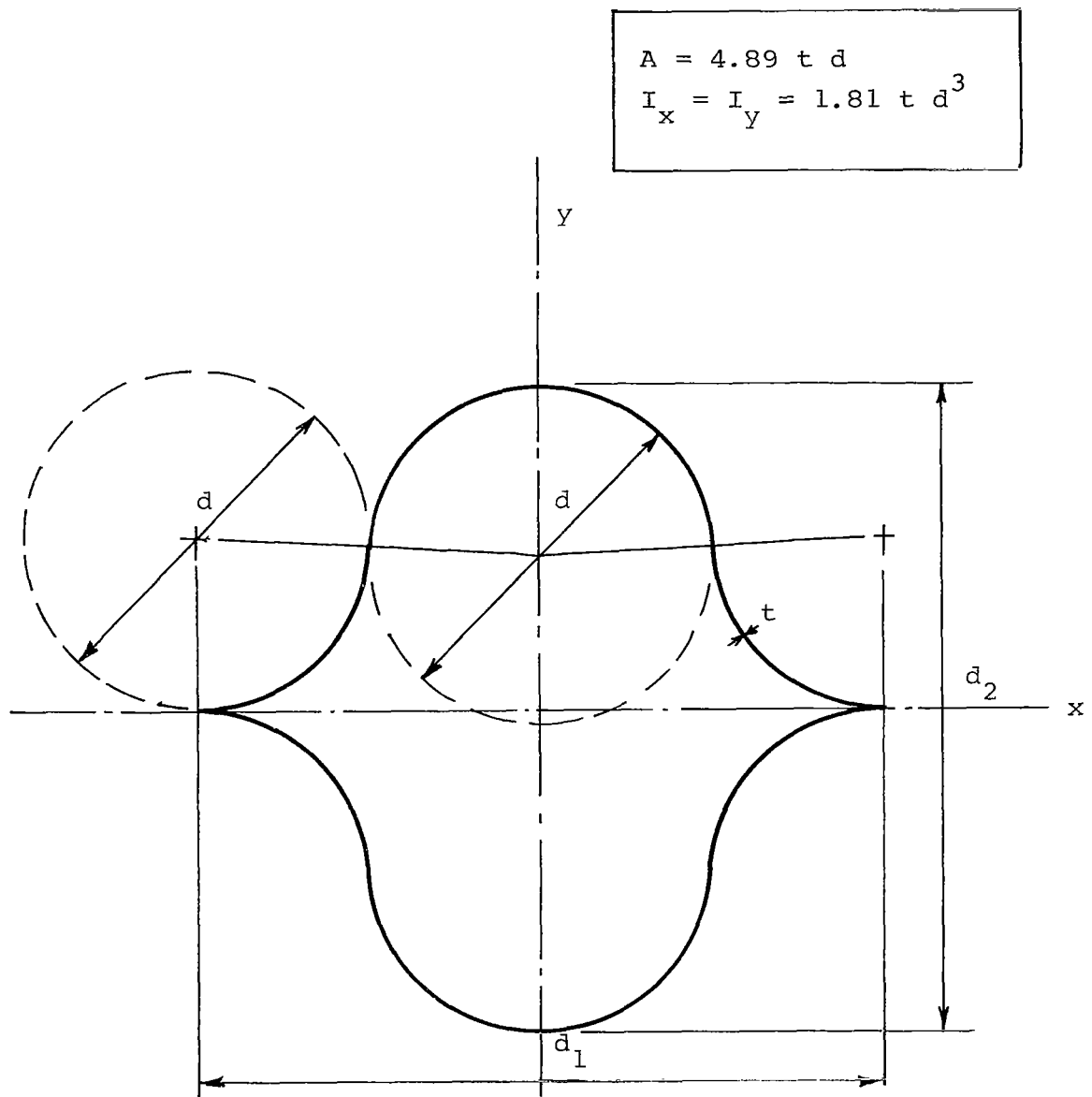
41

$$A = 4.89 \ t \ d$$
$$I_x = I_y = 1.81 \ t \ d^3$$

Figure 13.   Cross Section of Flattenable, Coilable "Sintes Tube"
for Moon Dome $(I_x = I_y)$

42

APPENDIX

GENERAL INSTABILITY OF DOME-SHAPED ISOSTABILOIDS

The lowest general instability mode of a dome-shaped iso-stabiloid may be determined approximately by replacing the network structure with an "equivalent" uniform shell of revolution. Solutions to shell buckling problems of this type are available in the published literature.

For a dome-shaped shell of uniform wall thickness, t_s, and subject to axial loading, the lowest instability failure mode seems to be inextensional, according to Reference 6, and it will generally exhibit meridional node lines (see inset of Figure A-1). The number of node lines, q, depends, among other parameters, on the wall thickness-to-semispan ratio of the shell, t_s/r_o. Figure A-1, derived from data of Reference 6, shows this dependence for the particular case of a paraboloidal dome with a meridional angle at the shell rim, α_o, of 45°.

Now, by defining an "equivalent" wall thickness for isosta-biloids the data of Reference 6 may be applied to these gridwork structures provided the meridional shapes of the shell and the isostabiloid are similar.

From inspection of the buckling mode it appears that the bending stiffness in circumferential direction is the dominant elastic shell property controlling the buckling mechanism. While the bending stiffness per unit transverse width of the isotropic shell is uniform

$$EI'_s = \frac{Et_s^3}{12(1-\nu^2)} \tag{A-1}$$

it varies with location and direction for an interconnected grid-work of rods, forming an isostabiloid, and becomes in the circumferential direction

$$EI'_c = EI \frac{n}{\pi r} \sin^3\beta \left(\tan\beta + \frac{GJ}{EI}\cot\beta\right) \tag{A-2}$$

43

EI and GJ are the bending stiffness and the torsional stiffness of a single straight rod.

The equivalent wall thickness of an isostabiloid, $\overline{t_{eq}}$ is now defined by combining equations (A-1) and (A-2) and integrating over the complete structure to obtain an average value

$$\overline{t_{eq}}^3 = 12(1-\nu^2)\, \frac{1}{r_o} \int_0^{r_o} I_c'\, dr$$

Using Eq. (5) to substitute r_o the equivalent wall thickness is found in its final general form as

$$\overline{t_{eq}}^3 = \frac{12(1-\nu^2)}{\pi} \left(n\frac{\rho g I^2 A}{CE}\right)^{1/3} \frac{1}{R_o} \int_0^{R_o} \frac{\sin^4\beta + \frac{GJ}{EI}\sin^2\beta}{R\cos\beta}\, dR \qquad (A-3)$$

For the special case where the structural members are made from circular tubing Eq. (A-3) reduces to

$$\overline{t_{eq}}^3 = \frac{12}{\pi} \left(n\frac{\rho g I^2 A}{CE}\right)^{1/3} \frac{1}{R_o} \int_0^{R_o} \frac{(1-\nu^2)\sin^4\beta + (1-\nu)\sin^2\beta}{R\cos\beta}\, dR$$

which, using $\nu = 0.3$, yields for the minimum weight configuration

$$(\overline{t_{eq}}^3)_{mw} = 0.231\,\frac{12}{\pi}\left(n\frac{\rho g I^2 A}{CE}\right)^{1/3}$$

Referring to Figure A-1, it can now be postulated that if $q \gtrless 2n$ then the corresponding isostabiloid will indeed fail in the assumed manner. If $q \lesssim n$ it may be suspected that the lowest instability mode of the corresponding isostabiloid involves motions of joints normal to the surface and that the isostabiloid design will not be valid, unless additional constraints (such as braces, stay wires, etc.) are used to prevent such failure modes.

The foregoing approximations must be used with caution since they do not account for unsymmetrical instability modes that may be caused by unavoidable geometrical imperfections and by side load components; nor do they account for failure modes that are associated with tangential strains.
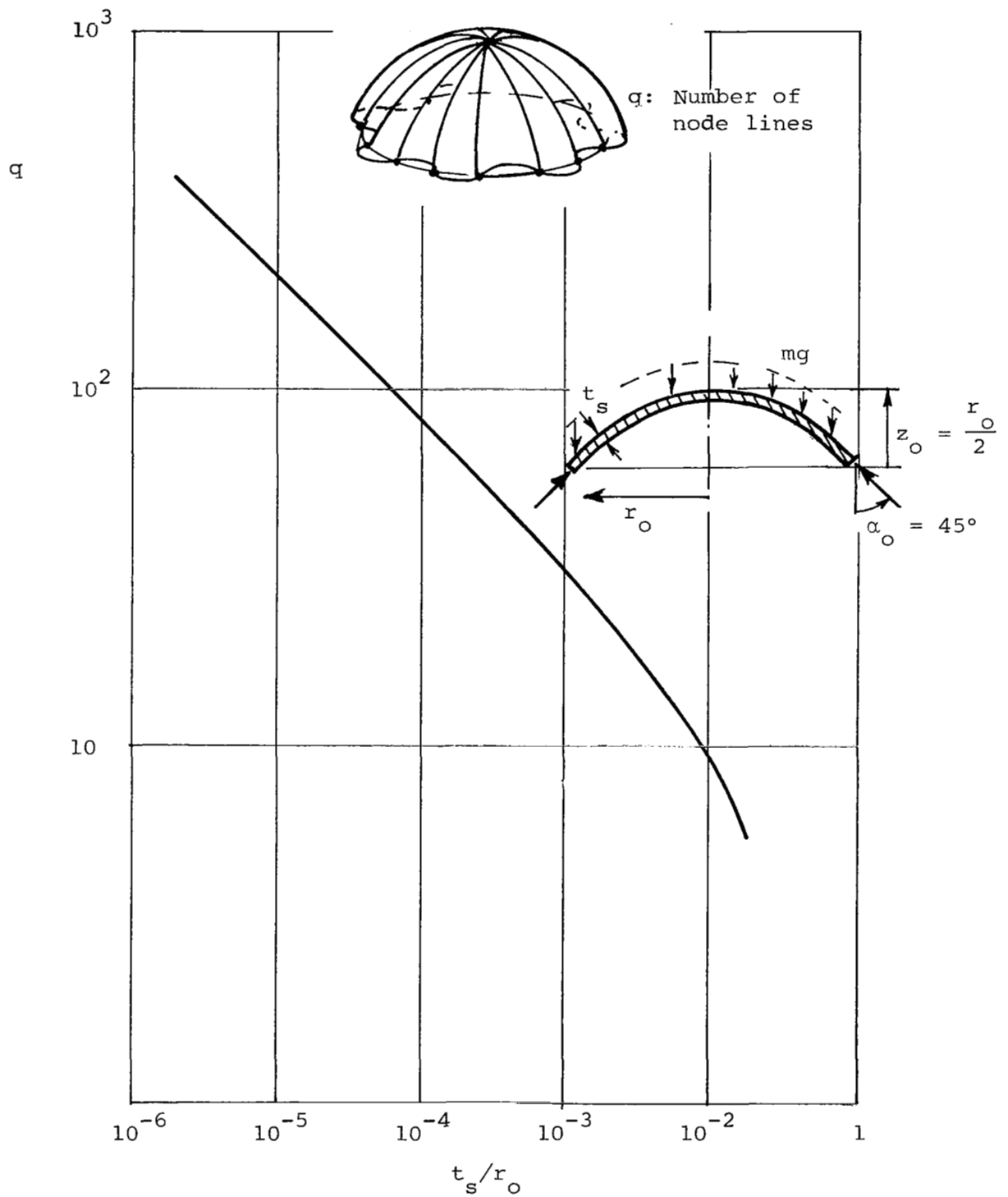
Figure A-1. Number of Meridional Node Lines for Lowest Buckling
Mode of Parabolic Dome Shell (Ref. 6)

REFERENCES

1. Schuerch, H.U. and Burggraf, O.R.: Analytical Design for Optimum Filamentary Pressure Vessels. AIAA Journal, Vol. 2, No. 5, May 1964.

2. Kyser, A.C.: The Uniform-Stress Spinning Filamentary Disk. NASA CR-106, October 1964.

3. Shanley, F.R.: Weight-Strength Analysis of Aircraft Structures. Dover, New York, 1960.

4. Fraser, A.F., et al: Axisymmetric Filamentary Structures. Astro Research Corporation, ARC-R-274, November 1968.

5. Sintes, J.F.: Flexural Instability of Foldable Tubes Based on the Elastic Recovery Concept. XVII Congress of the International Astronautical Federation, Madrid, Spain, October 1966.

6. Pfluger, A.: Stabilitaetsprobleme der Elastostatik. P. 294, Springer, Berlin, 1950.